Int J Earth Sci (Geol Rundsch) (2017) 106:1723–1733
DOI 10.1007/s00531-016-1381-5

ORIGINAL PAPER

S- and Sr-isotopic compositions in barite–silica chimney from the Franklin Seamount, Woodlark Basin, Papua New Guinea: constraints on genesis and temporal variability of hydrothermal fluid

Durbar Ray[1] · Ranadip Banerjee[1] · S. Balakrishnan[2] · Anil L. Paropkari[1] · Subir Mukhopadhyay[3]

Received: 27 August 2015 / Accepted: 1 August 2016 / Published online: 31 August 2016

Abstract Isotopic ratios of strontium and sulfur in six layers across a horizontal section of a hydrothermal barite–silica chimney from Franklin Seamount of western Woodlark Basin have been investigated. Sr-isotopic ratios in barite samples ($^{87}Sr/^{86}Sr$ = 0.70478–0.70493) are less radiogenic than seawater ($^{87}Sr/^{86}Sr$ = 0.70917) indicating that substantial leaching of sub-seafloor magma was involved in the genesis of hydrothermal fluid. The SO_2 of magma likely contributed a considerable amount of lighter S-isotope in fluid and responsible for the formation of barite, which is isotopically lighter ($\delta^{34}S$ = 19.4–20.5 ‰) than modern seawater ($\delta^{34}S$ ~ 21 ‰). The systematic changes in isotopic compositions across the chimney wall suggest temporal changes in the mode of mineral formation during the growth of the chimney. Enrichment of heavy S- and Sr-isotopes ($\delta^{34}S$ = 20.58 ‰; $^{87}Sr/^{86}Sr$ = 0.70493) in the outermost periphery of the chimney indicates that, at the initial stage of chimney development, there was a significant contribution of seawater sulfate during barite mineralization. Thereafter, thickening of chimney wall occurred due to precipitation of fluid carrying more magmatic components relative to seawater. This led to a gradual enrichment of lighter isotopes ($\delta^{34}S$ = 20.42–19.48 ‰; $^{87}Sr/^{86}Sr$ = 0.70491–0.704787) toward the inner portion of the chimney wall. In contrast, the innermost layer surrounding the fluid conduit is characterized by heavier and more radiogenic isotopes ($\delta^{34}S$ = 20.3 ‰; $^{87}Sr/^{86}Sr$ = 0.7049). This suggests there was increasing influence of percolating seawater on the mineral paragenesis at the waning phase of the chimney development.

Keywords Franklin Seamount · Woodlark Basin · Papua New Guinea · Hydrothermal barite–silica chimney · Sulfur isotope · Strontium isotope

Introduction

Barite, a common authigenic sulfate mineral of the marine environment, is reported to form in the water column as well as within sediment; especially around the cold seeps and hydrothermal vent fields (Griffith and Paytan 2012). Barite of hydrothermal origin develops mostly due to precipitation of Ba^{+2} rich fluids and is reported in several hydrothermal fields in different marginal basins, volcanic seamounts and oceanic ridges (Kusakabe et al. 1990; Stüben et al. 1994; Herzig et al. 1998; Paytan et al. 2002; de Ronde et al. 2003; Hein et al. 2007; Noguchi et al. 2011; Griffith and Paytan 2012; Eickmann et al. 2014). The Franklin Seamount in Woodlark Basin, off Papua New Guinea, is a large circular (diameter ~2.0 km) submarine volcano known for low-temperature (20–30 °C) hydrothermal activities (Lisitzin et al. 1997). This volcanic seamount hosts several barite–silica chimneys within its caldera (Binns et al. 1993, 1997; Bogdanov et al. 1997; Boyd and Scott 2001).

Previously, Binns et al. (1993, 1997) described the mineralogy and elemental chemistry of hydrothermal barite recovered from this seamount. The results showed that the relative abundances of barite, silica and sulfides differ

✉ Durbar Ray
dray@nio.org

[1] CSIR-National Institute of Oceanography, Dona Paula, Goa 403004, India

[2] Department of Earth Sciences, Pondicherry University, Puducherry 605014, India

[3] Department of Geological Sciences, Jadavpur University, Kolkata 700032, India

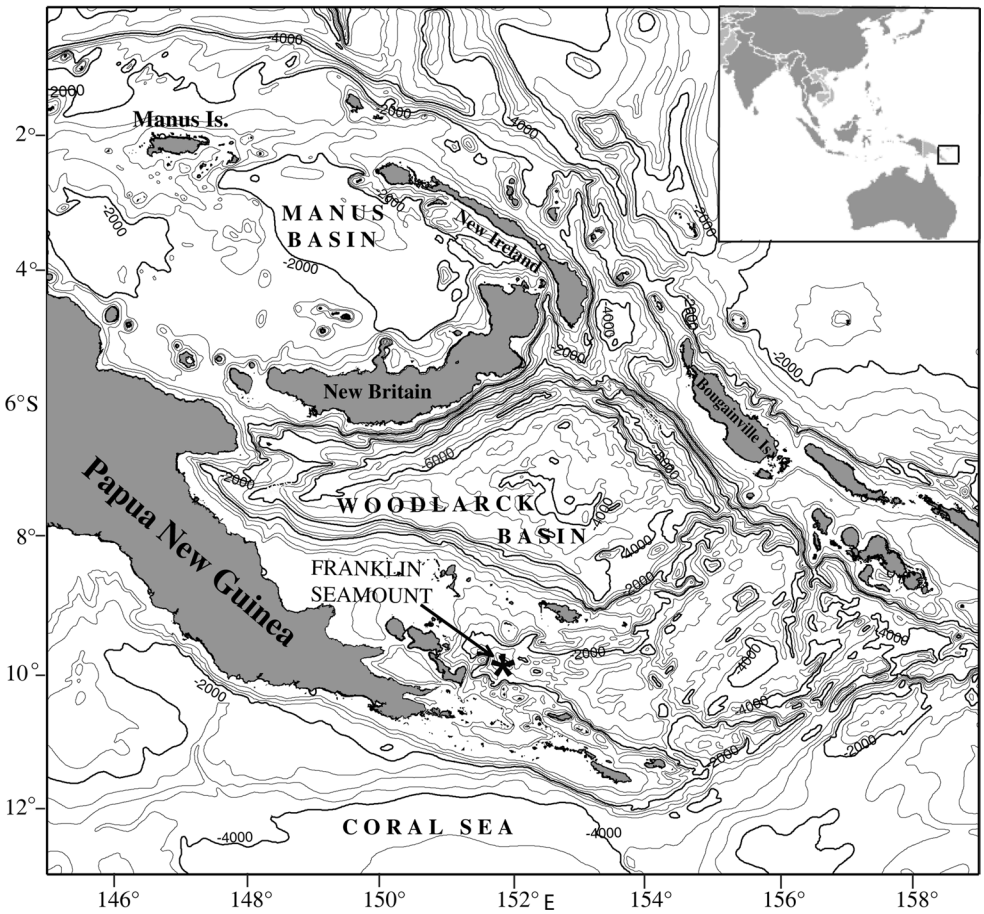

Fig. 1 Bathymetric map showing the location of Franklin Seamount in western Woodlark Basin off Papua New Guinea

significantly in these deposits. Ray et al. (2014) found that besides the relative abundance, textures of the minerals vary even within the individual chimneys. The same study suggested that episodic changes of hydrothermal fluid were responsible for such mineralogical variations.

Any temporal change in subsurface mixing of magma with seawater can alter the geochemical nature of the hydrothermal fluid (Paytan et al. 2002; Staude et al. 2011; George et al. 2013). This eventually results in distinct mineral zonings within individual deposits (Stüben et al. 1994; Tivey et al. 1995; Paropkari et al. 2010). Isotopic compositions of certain elements like sulfur and strontium which depend on the nature of source fluid are also expected to vary in different mineral zonings and would provide valuable information about the possible changes in fluid composition and/or the depositional environment.

In the present investigation, based on the isotopic composition of S and Sr in barite–silica chimney, certain issues linked to the genesis of hydrothermal fluid are discussed. Moreover, the most feasible temporal changes in fluid composition during the growth of the chimney are also inferred from the variations in mineralogy, elemental compositions and isotopic ratios in different parts of the chimney wall.

Materials and methods

Collection and brief description of sample

In 1990, under the multinational SUPACLARK (Soviet Union–Papua New Guinea–Australia–Canada) program, several hydrothermal fields of different marginal basins in the southwest Pacific Ocean were thoroughly explored and were sampled using *MIR* submersibles onboard *ORV Akademik Mstislav Keldysh*. During the *MIR-2* dives (dive nos. *M-2192* and *M-2202*), a number of barite–silica chimney structures of different heights rising from a mound-like base were found inside the caldera of Franklin Seamount (Fig. 1) (Binns et al. 1997). One extinct chimney was collected from the dive site, *M-2202* (09°54.45′S and 151°49.62′E) at the water depth of 2247 m.

A horizontal section from the top portion of the barite–silica chimney (*M-2202-1A2* in Fig. 2) was used for the present isotopic investigation. This chimney section has distinct mineral zonings characterized by variable abundance and crystal habits of barite, silica and metal sulfides (Ray et al. 2014). The outermost rim and the layer near the fluid orifice are made up of colloform silica and partly

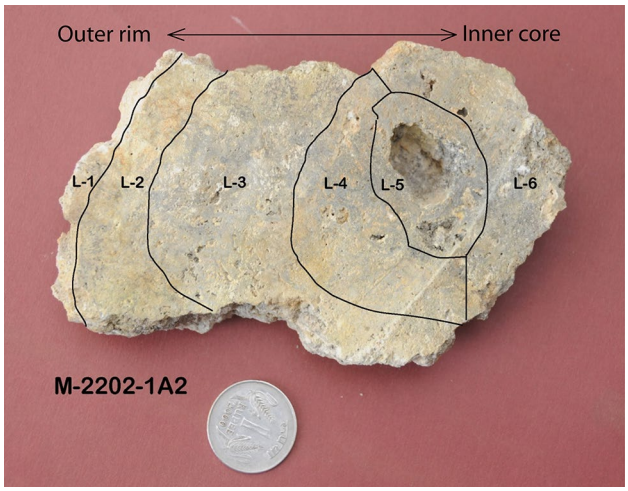

Fig. 2 Cross section of barite–silica hydrothermal chimney collected from the Franklin Seamount, Woodlark Basin. L1–L6 represent six layers of the chimney section, M2202-1A2, used for mineralogical and isotopic investigation. Diameter of the coin in this figure is 2.5 cm

crystalline barite, whereas the intermediate portion contains well-developed large euhedral barite crystals, silica and traces of disseminated metal sulfides (mostly pyrite) (Table 1; Ray et al. 2014).

Subsampling and analytical methods

To understand the sub-seafloor mechanism(s) involved in the evolution of hydrothermal fluid and its subsequent mineralization, S- and Sr-isotopic investigation was carried out in subsamples from different layers of the chimney wall. Accordingly, the horizontal section *M2202-1A2* of the barite–silica chimney was dissected into six subsamples (L1–L6) as shown in Fig. 2. These subsamples display minor variations in color which correspond to diverse mineral zonings within that chimney section (Ray et al. 2014). After separation, samples from each layer were washed thoroughly with Milli-Q® water to remove the absorbed salts and then dried in a hot-air oven. Several small chips (26 nos.) and polished samples from all six layers were thoroughly scanned with reflected light microscope and scanning electron microscope (JEOL JSM-5800LV) for textural and mineralogical analyses. A portion of each subsample was crushed into fine powder and used for other geochemical analyses. Bulk mineralogy and major element compositions in the powdered samples were determined with an XRD (Rigaku PW-1710) and an XRF (Axios PANalytical), respectively, at CSIR-National Institute of Oceanography, Goa.

Prior to isotopic analysis, barite and silica of chimney samples were separated from sulfides following the method modified after Noguchi et al. (2011). Finely powdered samples were heated with 50 % ultra-pure nitric acid (at 200 °C for 12 h) to dissolve the traces of metal sulfides. After acid digestion, the white residues were filtered out on 0.45-µm Millipore filters; washed with deionized water and dried at 110 °C. About 0.5 gm of fine barite–silica powder from each layer was thoroughly treated with 15 ml 0.1 (N) ultra-pure HCl followed by deionized water four times to remove all surface contamination. At each step, samples were sonicated and then supernatants were discarded. All subsamples were analyzed for Sr-isotopic ratio (i.e., $^{87}Sr/^{86}Sr$) following the modified leaching method described by McCulloch (1994). Cleaned samples were soaked in distilled water and sonicated at regular intervals for a week. Over this period, a significant amount of Sr (0.9–1.2 ppm) was leached out from all samples into the aqueous medium. Sr in aqueous supernatants was purified from other major ions by passing through a cation exchange column filled with Bio-Rad AG50-WX8 resin and then eluted with 2 (N) HCl. Thereafter, solutions were loaded onto single tungsten filaments with a TaF mixture and precisely analyzed in triplicate by using a thermal ionization mass spectrometer (TIMS, model: Triton Thermo Finnigan) at the Department of Earth Sciences, Pondicherry University. Sr-isotopic compositions are reported in terms of isotopic ratio, $^{87}Sr/^{86}Sr$. To assess the repeatability of the whole extraction process, samples from each layer were extracted in duplicate and analyzed separately (corresponding results are presented as A and B in Table 1). The accuracy and precision of TIMS measurements were evaluated against reference standard $SrCO_3$, SRM-987 from NIST, USA. After every sample, SRM-987 was analyzed and this yielded an average $^{87}Sr/^{86}Sr$ ratio of 0.710244 (± 0.000008; 2σ) against the certified value of 0.71034 ± 0.00026. The measured isotopic composition in SRM-987 is in good agreement with "accepted value" of 0.710263 ± 0.000016 reported in several literatures (Stein et al. 1997; Ehrlich et al. 2001).

Stable S-isotopic ratios were measured with a Europa Scientific 20–20 IRMS interfaced to a Roboprep elemental analyzer (Europa Scientific). Thoroughly cleaned sulfide-free dry finely powdered sample along with V_2O_5 in tin capsules was combusted at 1700 °C in a furnace. The combusted gases were then swept in a helium stream over combustion catalysts (tungstic oxide/zirconium oxide) and through a reduction stage of high-purity copper wire to produce SO_2, N_2, CO_2 and water. Moisture in the gas mixture was removed using a Nafion™ membrane. Then sulfur dioxide was resolved from N_2 and CO_2 on a packed GC column at a temperature of 45 °C. The resultant SO_2 gas was analyzed for isotopic composition with the IRMS at stable isotope laboratory of Iso-Analytical, UK. Isotopic abundances of sulfur are presented as $\delta^{34}S$ relative to Vienna Canyon Diablo Troilite (V-CDT), where

Table 1 Preliminary description and isotopic compositions of six layers in horizontal section of barite hydrothermal chimney from the Franklin Seamount, Woodlark Basin

Chimney layers	Thicker wall of the chimney section				Conduit	Thin wall
	Outer rim of the wall	Intermediate part of the wall between outermost rim and inner conduit			Layer around the conduit (L5)	Layer at another side of the conduit (L6)
	(L1)	(L2)	(L3)	(L4)		
Major minerals	col-si, br	br	br	br	col-si, br	br, col-si
Minor or trace minerals	–	col-si, ga, py	col-si, ga, asp, py	py, cp, mr, st, anh, col-si	msn, py, anh	msn
Na_2O (%)	0.6	0.7	0.7	0.6	0.6	0.7
CaO (%)	0.2	0.2	0.2	0.1	0.1	0.2
BaO (%)	40	40	42	38	39	44
SrO (%)	1.0	0.7	0.7	0.6	0.9	1.0
SiO_2 (%)	23	14	18	20	24	12
Al_2O_3 (%)	0.3	0.2	0.2	0.3	0.2	0.3
Fe_2O_3 (%)	18	18	19	18	18	19
MnO (%)	ND	0.8	0.7	ND	0.7	0.7
Cr_2O_3 (%)	7.0	7.0	7.0	7.0	7.0	8.0
NiO (%)	0.7	0.8	0.8	0.8	0.8	0.8
SO_3 (%)	8.0	17	11	13	9.0	11
As_2O_3 (%)	ND	0.02	0.01	0.01	ND	0.01
PbO (%)	ND	0.2	0.1	0.1	ND	0.1
Total	98.9	99.4	100.3	98.4	100.3	97.7
$\delta^{34}S_{VCDT}$ (‰)						
A	20.45	20.41	19.96	19.36	20.30	19.64
B	20.70	20.42	19.98	19.60	20.28	19.61
Average $\delta^{34}S$ (±2SE)	20.58 (0.12)	20.42 (0.01)	19.97 (0.01)	19.48 (0.11)	20.29 (0.01)	19.63 (0.02)
$^{87}Sr/^{86}Sr$ (2σ)						
A	0.705000 (1.1×10^{-5})	0.704899 (1.5×10^{-5})	0.704888 (1.4×10^{-5})	0.704878 (8.0×10^{-6})	0.704892 (9.0×10^{-6})	0.704804 (9.0×10^{-6})
B	0.704896 (5.0×10^{-6})	0.704918 (5.0×10^{-6})	0.704889 (6.0×10^{-6})	0.704879 (1.0×10^{-5})	0.704907 (5.0×10^{-6})	0.704769 (6.0×10^{-6})
Average $^{87}Sr/^{86}Sr$ (±2SE)	0.704948 (6.2×10^{-5})	0.704909 (9.5×10^{-5})	0.704888 (5.0×10^{-7})	0.704878 (5.0×10^{-7})	0.704900 (7.4×10^{-6})	0.704787 (1.7×10^{-5})

The mineralogy and major elements data are obtained from Ray et al. (2014)

col-si, colloform silica; br, barite; ga, galena; py, pyrite; anh, anhydrite; cp, chalcopyrite; msn, metasideronatrite; mr, marcasite; asp, arsenopyrite; st, strontianite

$\delta^{34}S_{V\text{-}CDT} = [\{(^{34}S/^{32}S)_{Sample\ or\ Standard}/(^{34}S/^{32}S)_{V\text{-}CDT}\} - 1]10^3$ (Coplen and Krouse 1998). A duplicate set of extraction and analyses of $\delta^{34}S_{V\text{-}CDT}$ (A and B in Table 1) restrict maximum standard error within a limit of ±0.12 ‰. The accuracy of instrumental measurement was evaluated against international reference standards IA-R061 and IAEA-SO5. Estimated $\delta^{34}S_{V\text{-}CDT}$ values of 20.23 ± 0.26 ‰ (1σ, $n = 03$) and 0.51 ± 0.06 ‰ (1σ, $n = 03$) were obtained for certified reference materials IA-R061 ($\delta^{34}S = 20.33$ ‰) and IAEA-SO5 ($\delta^{34}S = 0.5$ ‰), respectively.

Results and discussion

The mineralogy, major element composition and isotopic ratios of S and Sr of six subsamples of the barite–silica chimney section (*M-2202-1A2*) are summarized in Table 1. The results showed that similar to the elemental composition, the isotopic data of S and Sr have a considerable and systematic variation across the chimney section. The geochemical variations from the external rim to the inner fluid channel of the chimney indicate that there was a change in

the nature of parent fluid and/or formation mechanism with time during different phases of the chimney development.

Sulfur- and Strontium-isotope systematics: relative contributions of magma versus percolated seawater toward the generation of hydrothermal fluid

The measured sulfur isotopic ratios ($\delta^{34}S_{V\text{-}CDT}$) in barite from different parts of this chimney section have a range between 19.48 and 20.58 ‰ (Table 1). These values are lighter than typical diagenetic or cold-seep barites ($\delta^{34}S$ > 21–70 ‰) which commonly precipitate from Ba-rich pore fluids within sedimentary column, but lies within the limit reported for typical hydrothermal barites ($\delta^{34}S_{V\text{-}CDT}$ ~ 16–23 ‰) (Urabe and Kusakabe 1990; Herzig et al. 1998; Paytan et al. 2002; Eickmann et al. 2014). Baritic chimneys from other parts of the Franklin Seamount also had a similar range of S-isotopic ratio ($\delta^{34}S_{V\text{-}CDT}$ = 19.2–20.9 ‰; Binns et al. 1997).

Usually, S-isotopic composition of any barite deposit barely differs from that found with dissolved sulfate-S in the source fluid from which it precipitated (Kusakabe and Robinson 1977). Thus, hydrothermal barite precipitated due to direct influence of seawater should have S-isotopic composition comparable with that reported for modern seawater ($\delta^{34}S$ = 21 ‰; Rees et al. 1978) or slightly more. Subsurface microbial activities can lead to the formation of heavier sulfate-S-rich hydrothermal barite from entrained seawater (Eickmann et al. 2014). However, our present study shows the estimated S-isotopic ratios in barite (19.4–20.5 ‰) of all subsamples are marginally lighter than contemporary seawater ($\delta^{34}S$ = 21 ‰), suggesting that the sulfate-S in this barite–silica chimney was not fully contributed by dissolved sulfate in seawater. Such lighter isotopic composition can be explained by either subsurface mixing of seawater with ^{32}S-rich H_2S ($\delta^{34}S$ < 1.0–2.0 ‰) in high-temperature fluid prior to barite formation (Hannington and Scott 1988; Shanks 2001); alternatively, disproportionation of magmatic volatiles, SO_2, or leaching of rock can also yield lighter S-isotope-rich sulfate minerals in hydrothermal deposit (Ohmoto and Lasaga 1982; Herzig et al. 1998).

In previous studies, it has already been established that subsurface magmatic process plays a significant role in hydrothermal activities in the western Woodlark Basin (Laurila et al. 2012). Another model-based study by Martinez et al. (1999) also concluded that there is rift-induced shallow mantle convection beneath the crust of western Woodlark Basin. The Franklin Seamount, over the active spreading axis of that basin, would likely have a shallow magma chamber, which could supply magmatic fluid rich in volatiles. The relative abundance of major sulfur species in magmatic volatiles is a function of temperature, pressure and oxidation state of magma (Rye 2005). Commonly, under low-pressure condition, SO_2 gas is the dominating S-species in a shallow magma source (Gerlach and Casadevall 1983; Rye 2005). As the less dense volatile rich magmatic source ascends upward, at temperature <400 °C, dissolved SO_2 starts to condense at higher fO_2 and slowly disproportionate into sulfate and sulfides (Ohmoto and Lasaga 1982; Rye 2005; Seal 2006) through hydrolysis as follows:

$$4SO_2 + 4H_2O = 3H_2SO_4 + H_2S$$

Fractionation of the S-isotope associated with this equilibrium reaction between different S-species favors enrichment of heavier S-isotope in sulfate phase, leaving the lighter fraction in sulfides (Ohmoto and Rye 1979). The kinetic isotope effect of this equilibrium generates ample oxidized sulfate-S, which is characterized by $\delta^{34}S$ > 0 ‰ but is substantially lighter than dissolved sulfate in seawater (Herzig et al. 1998). This sulfate of magmatic origin can quantitatively react with available Ba in magma (and/or rocks) and precipitate as barite, which is isotopically lighter than seawater at relatively low temperature. Similar magmatic SO_2 oxidation has also been described for the evolution of sulfate minerals at different active hydrothermal fields in the adjacent basins (e.g., Snowcap site in Manus Basin, Roberts et al. 2003 and Hine Hina field on Lau back-arc spreading center, Herzig et al. 1998). Disproportionation of magmatic SO_2, as well as sulfides present in the magma, would generate H_2S in the upwelling fluid. A trace quantity of disseminated sulfide particles (mostly pyrite, Table 1; Figs. 3c, 4e, f) in intermediate layers of barite chimney also supports disproportionation reaction which simultaneously generates both sulfide and sulfate ions. However, this anticipated result can argue with previous water column observations which showed fluid expelled through Franklin Seamount contains no measurable dissolved H_2S (Binns et al. 1993; Lisitzin et al. 1997). Therefore, it can be argued that dissolved H_2S in the ascending fluid was completely consumed either through precipitation of metal sulfides on the deeper wall rock of fluid channel or through oxidation in shallow depths or through combination of these methods and thus made the expelled fluid free of traceable H_2S. Therefore, it is quite reasonable to assume that the mechanism involving sub-seafloor hydrolysis of magmatic SO_2 in shallow stock-work zone could be the main source for lighter S-isotope in this barite–silica chimney.

Besides sulfur isotopes, hydrothermal barite can also record Sr-isotopic composition of the parent fluids, and thus, the nature of fluid responsible for barite formation can be constrained from such isotopic investigations (Paytan et al. 2002; Noguchi et al. 2011; Griffith and Paytan 2012). Our results show $^{87}Sr/^{86}Sr$ ratio in this barite chimney has a range between 0.704787 and 0.704948 (Table 1). This estimated range is consistent with that found in barite from

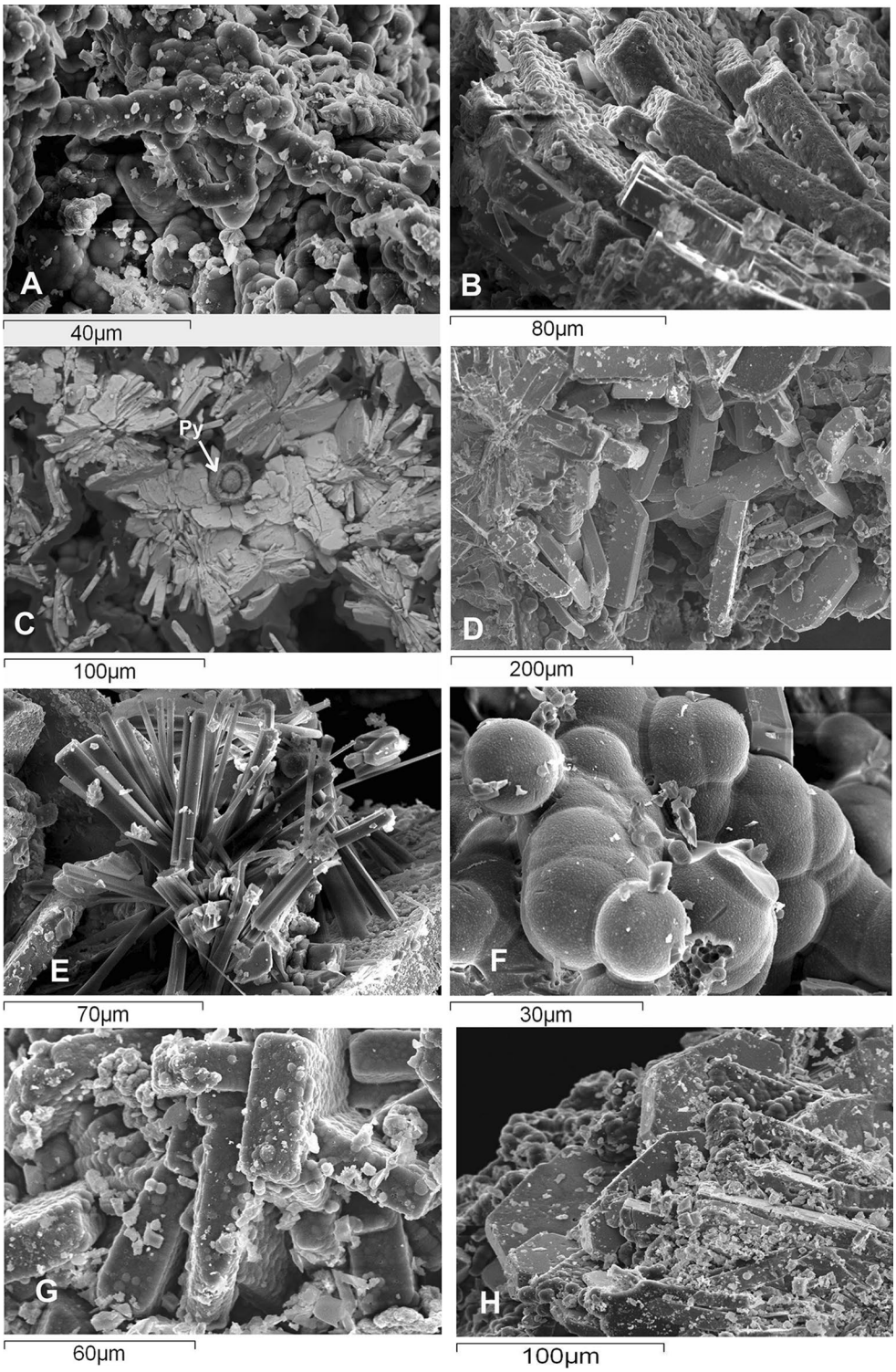

Fig. 3 SEM images of barite and silica deposit in different layers of chimney section, M2202-1A2. **a** Colloform silica with less barite in outermost layer, L1; **b** smaller bladed barite crystals with globular silica cover in layer, L2; **c** BSE image of rosette-shaped barite with an isolated framboidal pyrite (Py) crystal in layer, L3; **d** large prismatic and rectangular platy barite crystals in layer, L4; **e** radiated dendritic barite; **f** globular colloform silica in layer, L5; **g**, **h** platy barite crystals in layer, L6

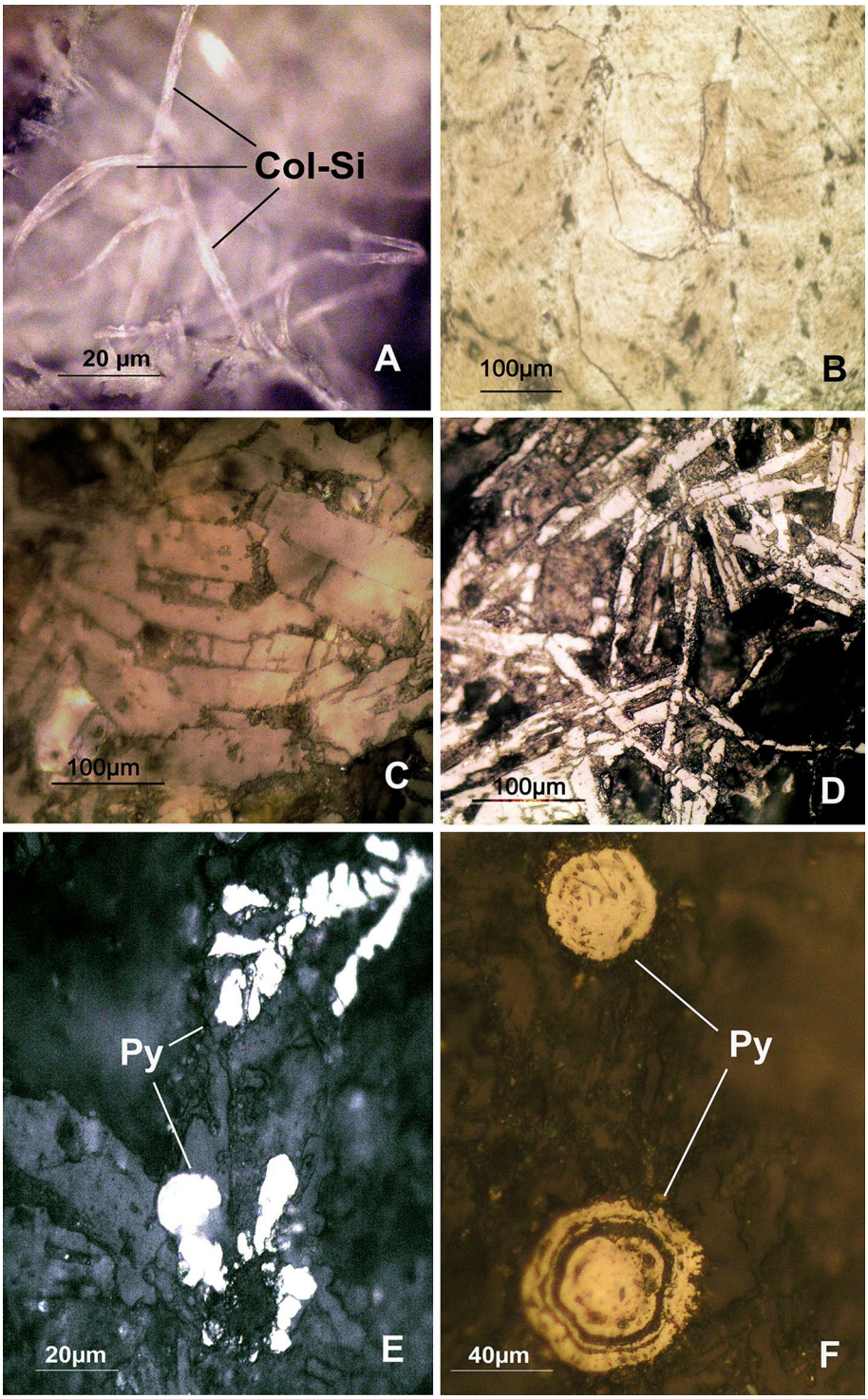

Fig. 4 Microscopic view of polished sections from different layers of barite–silica chimney section. **a** Filaments of colloform silica (Col-Si) in layer L1, **b** massive barite of layer L2, **c** larger platy barites from intermediate layer L3, **d** thin crosscutting needle-shaped barite from near orifice, L5, **e** framboidal pyrite and **f** spherical pyrites in intermediate layers L3 and L4, respectively

other parts of the Franklin Seamount ($^{87}Sr/^{86}Sr = 0.70481–0.70484$; Binns et al. 1997) as well as hydrothermal barites ($^{87}Sr/^{86}Sr < 0.706$; Fig. 5b) deposited in sediment-starved back-arcs and mid-oceanic ridges (Paytan et al. 2002; Noguchi et al. 2011). However, the observed isotopic ratios are lower than sediment-hosted hydrothermal barites ($^{87}Sr/^{86}Sr > 0.706$) precipitated with isotopic signature closer to modern seawater (Noguchi et al. 2011). Isotopic ratios in the barite–silica chimney of the present investigation have significantly less radiogenic ^{87}Sr relative to modern seawater ($^{87}Sr/^{86}Sr = 0.70917$, Fu and Aharon 1998); but the values were slightly more than those found in volcanic lava in western Woodlark spreading zone ($^{87}Sr/^{86}Sr = 0.7028–0.7039$; Binns et al. 1997) or basaltic andesites from Franklin

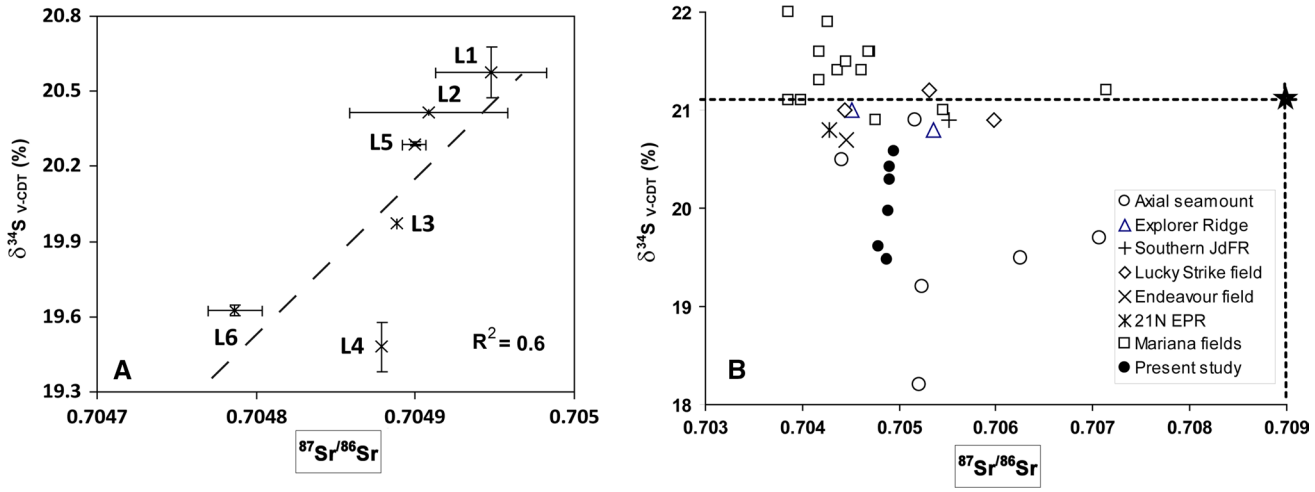

Fig. 5 Plots of S-isotopic composition vs. Sr-isotopic ratios. **a** Correlation between S- and Sr-isotopes in six layers of barite–silica chimney section, M2202-1A2. **b** The isotopic values of barite–silica chimney, M2202-1A2, from Franklin Seamount are compared with other known hydrothermal barites (Paytan et al. 2002). The *asterisk* (*) in this figure indicates average S- and Sr-isotopic composition of typical deep seawater

Seamount ($^{87}Sr/^{86}Sr$ = 0.7029–0.7032; Binns et al. 1993). Therefore, the estimated $^{87}Sr/^{86}Sr$ ratio (0.70478–0.7049) of this chimney samples suggests that the Sr in the hydrothermal fluid, involved in the formation of this chimney, was acquired from both magmatic fluid and percolated seawater. However, without the knowledge of isotopic composition of the fluid, it is difficult to estimate the actual contribution of each component. An earlier study showed that $^{87}Sr/^{86}Sr$ ratio decreases linearly in any hydrothermal fluid and related deposits as the contribution of Sr from pristine magmatic melt relative to seawater increases in hydrothermal fluid (Kusakabe et al. 1990). According to Kusakabe et al. (1990), hydrothermal barite with $^{87}Sr/^{86}Sr$ ratios ranging from 0.704787 to 0.704948 is estimated to have only ~20 % contribution of Sr from seawater; while the rest is of magmatic origin. Comparing the bulk Sr concentration in rocks with that in the end-member hydrothermal fluid, Binns et al. (1997) also concluded that there was about 25 % contribution of seawater in the hydrothermal fluid of Franklin Seamount. Therefore, based on observed isotopic composition of both S and Sr, it can be concluded that these elements in barite–silica chimney are mostly contributed by magmatic components as compared to seawater. The positive correlation (R^2 = 0.6) between average S- and Sr-isotopic ratios (Fig. 5a) in this chimney section also supports the findings.

Alterations of isotopic composition across the chimney section: effect of temporal changes in nature of hydrothermal fluid

In the present investigation, like bulk concentrations, the isotopic composition of both S and Sr systematically varies in six subsamples from the outer rim to the inner core of the barite chimney (Table 1). Commonly, such changes in average isotopic composition across the individual chimney wall can be explained by temporal variations in the composition of the hydrothermal fluid (Herzig et al. 1998). Therefore, the variation of $^{87}Sr/^{86}Sr$ ratio and sulfur isotope systematic among six subsamples (L1–L6 in Fig. 2) indicates that there were changes in mechanisms involved in fluid evolution and/or mode of hydrothermal precipitation at different growth phases of this barite–silica chimney.

The outermost layer of the chimney, L1, contained abundant colloform silica (Figs. 3a, 4a) with relatively less barite and was devoid of any sulfide minerals. This external silica-dominated layer (SiO_2 = 23 %, Table 1) indicates the growth of this chimney was initiated through precipitation of colloform silica (Ray et al. 2014) from a hydrothermal fluid which was reported to have very high concentration of dissolved silica (10–15 µg-atom/L, Lisitzin et al. 1997). A similar development of low-temperature hydrothermal silica structure is reported at "Topless Tower" in Mariana back-arc spreading center (Stüben et al. 1994). The average isotopic composition of layer L1, which is considered to have formed at the early stage of chimney development, has maximum enrichment of heavy sulfur ($\delta^{34}S_{V\text{-}CDT}$ = 20.58 ‰) and radiogenic strontium ($^{87}Sr/^{86}Sr$ = 0.704948) (Table 1) compared to the other inner layers. The presence of colloform silica and lack of large well crystalline barite in L1 suggest that incipient chimney growth started through rapid hydrothermal precipitation due to mixing of emerging fluid with ambient seawater. Such non-equilibrium rapid mineralization is expected to incorporate more seawater components, which perhaps

have resulted in the S- and Sr-isotopic ratios of barite in outermost layer, L1 ($\delta^{34}S = 20.58$ ‰; $^{87}Sr/^{86}Sr = 0.704948$) more close to the average seawater values ($\delta^{34}S = 21$ ‰; $^{87}Sr/^{86}Sr = 0.70917$).

The intermediate layers (i.e., L2, L3 and L4) between external rim, L1, and inner orifice, L5, mostly contain well-developed barites which include massive formation (Fig. 4b) as well as cluster of large (70 to >200 μm) platy (Figs. 3b, 4c), rectangular (Fig. 3d) or rosette-shaped (Fig. 3c) crystals. Abundance of colloform silica was relatively less; instead, several isolated crystals or patches of metal sulfides were found in all the three intermediate layers (Figs. 3c, 4e, f). Considering analytical uncertainty, the average isotopic composition of barite in these layers was found to have lighter S ($\delta^{34}S_{V\text{-}CDT} = 19.4$–$20.4$ ‰) and less radiogenic Sr ($^{87}Sr/^{86}Sr = 0.704787$–$0.704909$) isotopic composition (Table 1) as compared to that found in very initial growth layer, L1. Like intermediate layers, the layer L6, the possible concentric part of L4 (Fig. 2), at another side of the fluid orifice also had well-developed platy barite (Fig. 3g, h) and was characterized by low $\delta^{34}S_{V\text{-}CDT}$ (19.6 ‰) and $^{87}Sr/^{86}Sr$ ratio (0.704787). Therefore, all the intermediate layers which were formed during the main active phase of chimney development contained more sulfur ($SO_3 > 11$–17 %, Table 1); however, barites of these layers were relatively enriched with lighter S-isotopes. This clearly indicates there was sufficient supply of lighter sulfur in fluid during the main growth phase of the chimney. Increasing contribution of magmatic volatile SO_2 (relative to sulfate from seawater) toward barite mineralization would be accountable for such drop in $\delta^{34}S$ values in those intermediate layers of the chimney wall. Large euhedral barite crystals (40–80 μm) of the intermediate layers also suggest that mineralization took place at the higher temperature with limited influence of seawater. Furthermore, a comparison among these layers showed that the average S-isotopic ratio gradually drops toward orifice of the chimney section in the order of L2 > L3 > L4 ~ L6 (Table 1). This decreasing trend in S-isotopic ratio might be due to increased magmatic inputs relative to percolated seawater in hydrothermal circulation, as the chimney grew. During active phase, due to fast discharge, the ascending buoyant fluid would likely have a limited chance to mix with percolated water in the sub-seafloor environment. At the same time, thickening of the chimney wall along with its growth also reduces the wall porosity and thus restricts infiltration of seawater through the wall. Thus, lower mixing ratios of seawater to magmatic components in parent hydrothermal fluid perhaps develop barite with marginally lighter Sr-isotopic composition in the intermediate layers as compared to the outermost layer (L1). However, changes of Sr-isotopic composition among the intermediate layers were not very significant, but a marginal decreasing trend in average $^{87}Sr/^{86}Sr$ ratio (Table 1) toward the orifice was observed. This may be due to gradual reduction in seawater influence, as also evident from S-isotopic distribution.

Isotopic compositions of S and Sr of the innermost layer (L5) are characteristically different from other layers, L1–L4 and L6 as discussed above. This perhaps indicates major change in the nature of the parental fluid during formation of L5. This innermost layer (L5) encircled the partially clogged chimney orifice, might have developed at the waning phase of the chimney growth, and mineralized under cooler condition. At the end of the chimney development, as the hydrothermal activity reduced, more seawater would entrain, causing higher water–rock ratio in the resultant upwelling fluid. This was responsible for fast precipitation of dendritic barites (Figs. 3e, 4d) and colloform silica (Fig. 3f) in this layer (Ray et al. 2014). Similar fast mineralization process involving more seawater components might be responsible for the substantial increase in heavier S-isotopic composition ($\delta^{34}S_{V\text{-}CDT} = 20.3$ ‰) in L5. Dilution of hydrothermal fluid with radiogenic Sr-rich seawater also would likely increase the Sr-isotopic ratio to a higher value ($^{87}Sr/^{86}Sr = 0.7049$), as found in this layer. Thus, S- and Sr-isotopic distributions helped to identify three-growth-phase history for barite–silica chimney which further corroborates with the earlier findings on growth mechanisms (Ray et al. 2014) of this chimney sample.

The plot of average Sr-isotopic ratios of six layers against their Si contents revealed a positive slope ($R^2 = 0.47$; Fig. 6a), while an inverse relation ($R^2 = 0.4$) was found with corresponding Ba concentrations (Fig. 6b). These relations suggest the variation of relative abundance barite and silica at different layers of the chimney altered with Sr-isotopic composition and therefore was probably influenced by fluid–seawater mixing ratios. More mixing of seawater would likely restrict barite precipitation, possibly through dilution of Ba in ascending fluid. However, the positive relation of Sr with SiO_2 suggests silica precipitation continued in spite of dilution with seawater, this could be due to two reasons: First, sufficient concentration of dissolved silica in both fluid and seawater is expected to limit the dilution effect for silica as compared to Ba. Second, the depletion of temperature during mixing with seawater helped the fluid to attain saturation with respect to silica and that favored precipitation of more colloform silica (Ray et al. 2014). Therefore, the small-scale isotopic variation across the chimney wall distinctly reveals three major growth phases of this chimney which include: (1) initial development of silica-rich outskirts of chimney wall (L1); (2) gradual thickening of wall on either side of the conduit

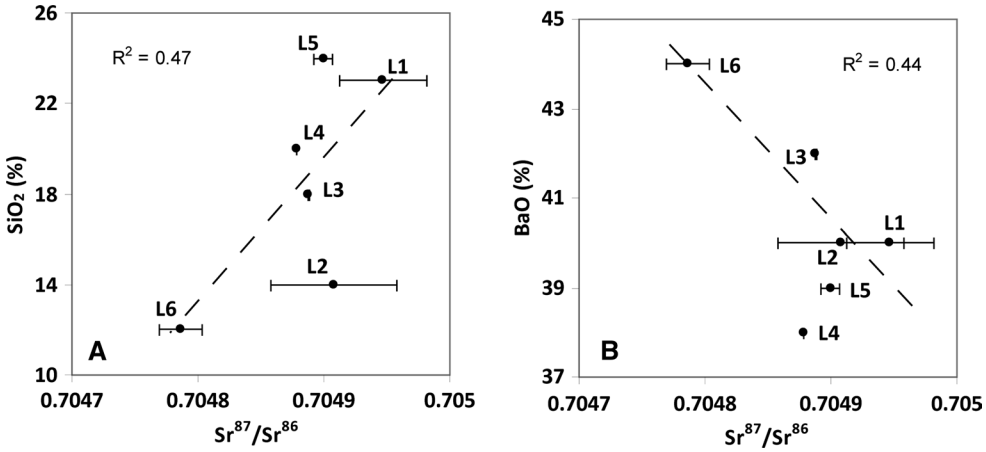

Fig. 6 Plots for Sr-isotopic ratios against **a** bulk barium and **b** silica contents in six layers of the barite–silica chimney, M2202-1A2

(L2, L3, L4 and L6) during active regime of the chimney; and (3) last phase of silica mineralization inside the conduit (L5) at the cooling stage of the chimney.

Conclusions

Integrated results of S- and Sr-isotopic compositions in the barite–silica chimney from the Franklin Seamount indicate subsurface magmatic components had dominant contribution as compared to percolated seawater toward the genesis of hydrothermal fluid. Oxidation of sulfur dioxide in shallow magma was the principal source for sulfate-S in that source fluid. Nevertheless, the observed fine-scale isotopic changes were found to be associated with separate mineral zonings across the chimney wall, which confirm that there were changes in fluid composition during the course of chimney growth. Such temporal variations in fluid occurred mostly due to change in contribution of seawater relative to the magmatic component in the source fluid. Thus, based on the distribution of minerals, element and isotopic compositions, the paragenesis in the chimney growth can be classified into three phases which include initiation of chimney development with silica deposition followed by its further growth through precipitation of sulfate and sulfide minerals and finally again silicification as the chimney lost its activity.

Acknowledgments Authors are thankful to the Director, CSIR-National Institute of Oceanography, Goa, for his permission to publish this work. Dr. A. L. Paropkari is grateful to Prof. A. P. Lisitzin for inviting him to participate in the 21st cruise of *ORV Keldysh* and providing samples to undertake scientific investigations. Thanks to Dr. J. K. Dash, Pondicherry University, and Mr. Khedekar, CSIR-NIO, Goa, for their help during TIMS and SEM analyses, respectively. This work was carried out under "GEOSINK" project funded by CSIR, India. Dr. S. Mukhopadhyay acknowledges DST-PURSE (Phase-II) funding for his work. Two anonymous reviewers and Dr. S. D. Iyer are thanked for their insightful comments on this manuscript. This is CSIR-NIO contribution no. 5929.

References

Binns RA, Scott AD, Bogdanov YA, Lisitzin AP, Gordeev VV, Gurvich EG, Finlayson EJ, Boyd T, Dotter IE, Wheller GE, Muravyev KG (1993) Hydrothermal oxide and gold-rich sulfate deposits of Franklin Seamount, western Woodlark Basin, Papua New Guinea. Econ Geol 88:2122–2153

Binns RA, Parr JM, Gemmell JB, Whitford DJ, Dean JA (1997) Precious metals in barite–silica chimneys from Franklin Seamount, Woodlark Basin, Papua New Guinea. Mar Geol 142:119–141

Bogdanov YA, Lisitzin AP, Binns RA, Gorshkov AI, Gurvich EG, Dritz VA, Dubinina GA, Bogdanova OY, Sivkov AV, Kuptsov VM (1997) Low-temperature hydrothermal deposits of Franklin Seamount, Woodlark Basin, Papua New Guinea. Mar Geol 142:99–117

Boyd TD, Scott SD (2001) Microbial and hydrothermal aspects of ferric oxyhydroxides and ferrosic hydroxides: the example of Franklin Seamount, Western Woodlark Basin, Papua New Guinea. Geochem Trans. doi:10.1186/1467-4866-2-45

Coplen TB, Krouse HR (1998) Sulphur isotope data consistency improved. Nature 392:32

de Ronde CEJ, Faure K, Bray CJ, Chappell DA, Wright IC (2003) Hydrothermal fluids associated with seafloor mineralization at two southern Kermadec arc volcanoes, offshore New Zealand. Mineral Deposita 38:217–233

Ehrlich S, Gavrieli I, Dor L, Halicz L (2001) Direct high-precision measurements of the $^{87}Sr/^{86}Sr$ isotope ratio in natural water, carbonates and related materials by multiple collector inductively coupled plasma mass spectrometry (MC-ICP-MS). J Anal Atom Spectrom 16:1389–1392

Eickmann B, Thorseth IH, Peters M, Strauss H, Bröcker M, Pedersen RB (2014) Barite in hydrothermal environments as a recorder of subseafloor processes: a multiple-isotope study from the Loki's Castle vent field. Geobiol 12:308–321

Fu B, Aharon P (1998) Sources of hydrocarbon-rich fluids advecting to the seafloor in the northern Gulf of Mexico. Trans Gulf Coast Assoc Geol Soc 48:73–82

George BG, Shalini N, Pandian MS, Rai VK, Bhutani R, Balakrishnan S (2013) Strontium and sulfur isotope constraints on the formation of the Mangampeta barite deposit, Cuddapah Basin. Curr Sci 104:499–504

Gerlach TE, Casadevall TJ (1983) Fumarole emissions at Mount St. Helens volcano, June 1980 to October 1981. Degassing of a magma–hydrothermal system. J Volcanol Geotherm Res 28:141–160

Griffith EM, Paytan A (2012) Barite in the ocean – occurrence, geochemistry and palaeoceanographic applications. Sedimentology 59:1817–1835

Hannington MD, Scott SD (1988) Mineralogy and geochemistry of a hydrothermal silica-sulfide-sulfate spire in the caldera of Axial-Seamount, Juan de Fuca Ridge. Can Mineral 26:603–625

Hein JR, Zierenberg RA, Maynard JB, Hannington MD (2007) Multifarious barite-forming environments along a rifted continental margin, Southern California Borderland. Deep Sea Res II 54:1327–1349

Herzig PM, Hannington MD, Arribas A Jr (1998) Sulfur isotopic composition of hydrothermal precipitates from the Lau back-arc: implications for magmatic contributions to seafloor hydrothermal systems. Mineral Deposita 33:226–237

Kusakabe M, Robinson BW (1977) Oxygen and sulfur isotope equilibria in the $BaSO_4$–H_2SO_4–H_2O system from 110° to 350°C and applications. Geochim Cosmochim Acta 41:1033–1040

Kusakabe M, Mayeda S, Nakamura E (1990) S, O and Sr isotope systematics of active vent materials from the Mariana backarc basin spreading axis at 18°N. Earth Planet Sci Lett 100:275–282

Laurila TE, Petersen S, Devey CW, Baker ET, Augustin N, Hannington MD (2012) Tectonic and magmatic control on hydrothermal activity in the Woodlark Basin. Geochem Goephys Geosyst 13:1–13

Lisitzin AP, Lukashin VN, Gordeev VV, Mcconachy TF, Scott SD, Shevchenko VP (1997) Hydrological and geochemical anomalies associated with hydrothermal activity in SW Pacific marginal and back-arc basins. Mar Geol 142:7–45

Martinez F, Taylor B, Goodliffe A (1999) Contrasting styles of seafloor spreading in the Woodlark Basin: indications of rift-induced secondary mantle convection. J Geophys Res 104:12909–12926

McCulloch MT (1994) Primitive $^{87}Sr/^{86}Sr$ from an Archean barite and conjecture on the Earth's age and origin. Earth Planet Sc Lett 126:1–13

Noguchi T, Shinjo R, Ito M, Takada J, Oomori T (2011) Barite geochemistry from hydrothermal chimneys of the Okinawa Trough: insight into chimney formation and fluid/sediment interaction. J Miner Petrol Sci 106:26–35

Ohmoto H, Lasaga AC (1982) Kinetics of reactions between aqueous sulfates and sulfides in hydrothermal system. Geochim Cosmochim Acta 46:1727–1745

Ohmoto H, Rye RO (1979) Isotopes of sulfur and carbon. In: Barnes HL (ed) Geochemistry of hydrothermal ore deposits, 2nd edn. Wiley, New York, pp 509–567

Paropkari AL, Ray D, Balaram V, SuryaPrakash L, Mirza IH, Satyanarayana M, GnaneshwarRao T, Kaisary S (2010) Formation of hydrothermal deposits at Kings Triple Junction, northern Lau back-arc basin, SW Pacific: the geochemical perspectives. J Asian Earth Sci 38:121–130

Paytan A, Mearon S, Cobb K, Kastner M (2002) Origin of marine barite deposits: Sr and S isotope characterization. Geol 30:747–750

Ray D, Kota D, Das P, Surya Prakash L, Khedekar VD, Paropkari AL, Mudholkar AV (2014) Microtexture and distribution of minerals in hydrothermal barite–silica chimney from the Franklin Seamount, SW Pacific: constraints on mode of formation. Geol Sin Acta 88:213–225

Rees CE, Jenkins WJ, Monster J (1978) The sulphur isotopic composition of ocean water sulphate. Geochim Cosmochim Acta 42:377–381

Roberts S, Bach W, Binns RA, Vanko DA, Yeats CJ, Teagle DAH, Blacklock K, Blusztajn JS, Boyce AJ, Cooper MJ, Holland N, McDonald B (2003) Contrasting evolution of hydrothermal fluids in the PACMANUS system, Manus Basin: the Sr and S isotope evidence. Geol 31:805–808

Rye RO (2005) A review of the stable-isotope geochemistry of sulfate minerals in selected igneous environments and related hydrothermal systems. Chem Geol 215:5–36

Seal RR (2006) Sulfur isotope geochemistry of sulfide minerals. Rev Mineral Geochem 61:633–677. doi:10.2138/rmg.2006.61.12

Shanks WC III (2001) Stable isotopes in seafloor hydrothermal systems: vent fluids, hydrothermal deposits, hydrothermal alteration, and microbial processes. In: Valley JW, Cole DR (eds) Stable isotope geochemistry. Reviews in mineralogy and geochemistry, vol 43. Mineralogical Society of America and the Geochemical Society, Washington, DC, pp 469–525

Staude S, Göb S, Pfaff K, Ströbele F, Premo WR, Markl G (2011) Deciphering fluid sources of hydrothermal systems: a combined Sr and S-isotope study on barite (Schwarzwald, SW Germany). Chem Geol 286:1–20

Stein M, Starinsky A, Katz A, Goldstein SL, Machlus M, Schramm A (1997) Strontium isotopic, chemical, and sedimentological evidence for the evolution of Lake Lisan and the Dead Sea. Geochim Cosmochim Acta 61:3975–3992

Stüben D, Taibi NE, Mcmurtry GM, Scholten J, Stoffers P, Zhang D (1994) Growth history of a hydrothermal silica chimney from the Mariana back-arc spreading center (southwest Pacific, 18°13′N). Chem Geol 113:273–296

Tivey MK, Humphris SE, Hannington MD, Rona PA, Thompson G (1995) Deducing patterns of fluid flow and mixing within the TAG active hydrothermal mound using mineralogical and geochemical data. J Geophys Res 100:12527–12555

Urabe T, Kusakabe M (1990) barite–silica chimneys from the Sumisu rift, Izu-Bonin arc: possible analog to hematitic chert associated with Kuroko deposits. Earth Planet Sci Lett 100:283–290